The effect of plasma sheet ion composition on the production and evolution of cold H^+ population from the hydrogen geocorona in the inner magnetosphere

Jianghuai Liu[1], Raluca Ilie[1], Joseph E Borovsky[2], Michael W Liemohn[3]

[1]Department of Electrical and Computer Engineering, University of Illinois at Urbana-Champaign, Urbana, IL, USA
[2]Space Science Institute, Boulder, CO, USA
[3]Department of Climate and Space Science and Engineering, University of Michigan, Ann Arbor, USA

Key Points:

- Ring current heavy ions (O^+ and N^+) can be responsible for a large portion of charge-exchange byproduct cold H^+.
- The charge-exchange byproduct cold H^+ have the potential to reshape the plasmasphere and enhance the early-stage plasmaspheric refilling.
- The cold H^+ contribution structure in the inner magnetosphere is primarily determined by the composition of energetic heavy ions.

Corresponding author: Jianghuai Liu, jliu115@illinois.edu

Abstract

Both in situ measurements and numerical simulations show that the charge exchange collisions between energetic ring current ions (>10keV) and cold ambient neutral atoms of the upper atmosphere and exosphere (<1eV) can be a major loss process of the ring current ions. Owing to the high volume of energetic ion source injected from the ion plasma sheet during storm time under strong convection strength, there can be a significant rate of occurrence of charge exchange collision in the inner magnetosphere, therefore contributing a significant amount of inner magnetospheric cold proton populations. Due to the different charge exchange cross sections among different reactions, cold protons are generated at different rates from different energetic ion species. In this study, both qualitative and quantitative assessments on the production and evolution of charge-exchange byproduct cold protons are performed via numerical simulations, showing that the production and evolution of the cold H^+ populations can be primarily driven by the plasma sheet conditions combined with the magnetospheric convection, while having the potential to affect the dynamics of the plasmasphere and facilitate the early-stage local plasmaspheric refilling. Furthermore, the energetic heavy ions composition plays an important role determining the cold H^+ contribution structure from the energetic ring current ions.

Plain Language Summary

The accumulation and intensification of energetic charged particles in the near-Earth space is an important aspect of space weather, especially space storms. The hot ions, while drifting in the near-Earth space, can collide with ambient low-energy neutrals, snatching an electron and therefore becoming neutral. The low-energy neutrals consequently lose an electron and become low-energy ions, and this electron swap between fast and cold particles is called charge exchange. This study addresses the role and contribution of energetic heavy ions on producing the cold protons due to these charge exchange reactions, and presents both qualitative and quantitative evaluations on the time-evolution of charge-exchange byproduct cold protons under different storm conditions. This study shows that energetic heavy ions can produce a significant amount of cold protons and therefore have profound impact on the cold charged particle populations.

1 Introduction

The terrestrial magnetospheric environment comprises plasma populations with a wide range of energy profiles, spanning from the sub-eV and eV particles of the ionosphere and plasmasphere, up to the ultra-relativistic energies of the radiation belts particles. These diverse plasma populations with different energies coexist, interact, and exchange energy with each other by means of a variety of collisional and wave-particle interactions (Liemohn, 2006; Yu et al., 2019). The detection of cold plasma populations is significantly impacted by spacecraft charging and secondary-electron contamination, which make reliable measurements of the cold ion populations and their analysis difficult (e.g. (Moore et al., 1997; Mozer et al., 2016; Genestreti et al., 2017; Gershman et al., 2017; Delzanno et al., 2021)). The main source of the magnetospheric cold plasma is the ionosphere (both low-latitude and high-latitude) where cold ion outflows are commonly observed (Coley et al., 2003; Andersson et al., 2004; Haaland et al., 2015; Artemyev et al., 2020; Dandouras, 2021), which can become the dominant source of magnetospheric hot plasma (Chappell et al., 1987; Winglee, 2000; Huddleston et al., 2005; Glocer et al., 2009; Welling & Ridley, 2010; Brambles et al., 2010; Welling, André, et al., 2015). There is growing evidence that supports the hypothesis that the cold-particle populations of the magnetosphere play critical roles in several important processes that drive the dynamics of the region (Winglee et al., 2002; Wiltberger et al., 2010; Brambles et al., 2011; Borovsky et al., 2013; Ouellette et al., 2013; Welling, Jordanova, et al., 2015; Trung et al., 2019; Delzanno et al.,

2021). As a result, understanding the origin, properties, drivers and impacts of cold-particle populations is a key factor of fully understanding the magnetosphere–ionosphere system.

While the cold-particle populations are sourcing a significant portion of magnetospheric hot-particle populations, hot-particle populations can also become the source of cold-particle populations via collisional charge exchange processes with regional neutral atoms (e.g. (Borovsky et al., 2022)). Due to the spatial overlap of the inner magnetospheric ion plasma sheet with the Earth's neutral hydrogen exosphere or the hydrogen geocorona (Carruthers et al., 1976; Rairden et al., 1986), charge exchange collisions between the low-energy geocoronal neutral hydrogen (less than one eV) and the ring current energetic ions (10's of keV) take place, as the energetic ions convect into the inner magnetosphere and undergo magnetic gradient-curvature drift. During the charge exchange process, the incident ring current ion picks up the orbital electron of a cold geocoronal hydrogen atom, resulting in the formation of an Energetic Neutral Atom (ENA) along with a byproduct low-energy proton. Borovsky et al. (2022) argues that the byproduct protons are produced at very low energies (sub-eV), which then become trapped by the geomagnetic field and advect with $\vec{E}\times\vec{B}$ drift, but possess too low energy to contribute to the ring current. Therefore, charge exchange with the neutral geocorona is an import loss process that accounts for some of the decay of the ring current intensity (Smith & Bewtra, 1978; Kistler et al., 1989; Liemohn et al., 1999; Liemohn & Kozyra, 2003, 2005; Ilie et al., 2013; Ilie & Liemohn, 2016), creation of unstable hot-ion distribution in the ring current region (Cornwall, 1977; Thomsen et al., 2011, 2017), and may also shorten the early-phase of the plasmaspheric refilling (Sojka & Wrenn, 1985; Su et al., 2001; Obana et al., 2010; Denton & Borovsky, 2014). The density of neutral hydrogen increases strongly approaching the Earth (e.g. (Chamberlain, 1963; Ilie et al., 2013; Borovsky et al., 2022)), therefore the probability of charge exchange increases greatly as an energetic ion approaches the Earth, consequently the byproduct cold protons of charge exchange are more likely to be produced at high altitudes and latitudes (Denton et al., 2005; Keika et al., 2006; He et al., 2015; Borovsky et al., 2022). The details of cold proton production depend on the energy profile, equatorial temperature distribution ($T_\perp/T_\parallel$), convection pattern, and ion composition of the hot plasma. If the trapped ring current hot ions are relatively isotropic on the equatorial plane, then there can be a significant amount of hot ions that mirror at high latitudes within the geosynchronous orbit (Denton et al., 2005; Denton et al., 2016), where the geocoronal neutral density is higher, therefore having the largest probability to undergo charge exchange. In addition, due to the different charge exchange cross section for reactions involving various ring current species with neutral hydrogen, changes in the regional ion composition can lead to changes in the cold proton population formed via the charge exchange interaction. Both numerical simulations and in situ measurements indicate that the ring current hot ion composition changes drastically depending on the solar wind and geomagnetic activity, while the heavy ions (primarily N^+ and O^+) can share a significant portion of ring current hot ions during storm time (Hultqvist, 1979, 1982; Fu et al., 2001; Kozyra et al., 2002; Orsini, 2004; Zhao et al., 2015; Ilie et al., 2015; Kistler & Mouikis, 2016; Lee et al., 2021; James et al., 2021). However, the particular effects and rates of energetic ring current heavy ions on producing charge-exchange byproduct cold protons have not been yet comprehensively assessed.

In this study, we evaluate the production of cold protons via charge-exchange reactions with energetic ring current ions. We present qualitative and quantitative estimations of the generation and time-evolution of these cold protons, with a special focus on those produced by heavy ions, based on numerical simulation using the Hot Electron-Ion Drift Integrator (HEIDI) model. Because plasmaspheric refilling may also be attributed to the charge exchange processes between energetic ions and the neutral hydrogen geocorona (Dessler et al., 1961; Milillo et al., 1996; Lawrence et al., 1999), the associated effects on the plasmaspheric refilling are also discussed.

2 Methodology

The HEIDI model is an inner magnetosphere kinetic drift model that solves the time-dependent, gyration- and bounce-averaged Boltzmann equation for the equatorial phase-space distribution function $F(t, \mathbf{r}_0, \mathbf{v}_0)$ of five ring current species (e^-, H^+, He^+, N^+, O^+). The model adopts an equatorial computation domain in space, discretized uniformly both in the radial and azimuthal directions, and is capable of handling arbitrary electric and magnetic fields. The bounce-averaged kinetic equation solved is (Liemohn et al., 2004; Ilie et al., 2012):

$$\frac{\partial F}{\partial t} + \frac{1}{R_0^2}\frac{\partial}{\partial R_0}\left(R_0^2 \left\langle \frac{dR_0}{dt} \right\rangle F\right) + \frac{\partial}{\partial \phi_0}\left(\left\langle \frac{d\phi_0}{dt} \right\rangle F\right) + \frac{1}{\sqrt{W}}\frac{\partial}{\partial W}\left(\sqrt{W}\left\langle \frac{dW}{dt} \right\rangle F\right) + \frac{1}{h(\mu_0)\,\mu_0}\frac{\partial}{\partial \mu_0}\left(h(\mu_0)\,\mu_0 \left\langle \frac{d\mu_0}{dt} \right\rangle F\right) = \left\langle \frac{\delta F}{\delta t} \right\rangle_{collision} + \left\langle \frac{\delta F}{\delta t} \right\rangle_{source} \tag{1}$$

Equation 1 describes the time-evolution of the phase-space distribution function at a certain location $(\mathbf{r}_0, \mathbf{v}_0)$ within the equatorial configuration-velocity space, under the effect of drifts, energization, pitch-angle scattering, and various loss mechanisms. Ring current losses include Coulomb collisions, charge exchange reactions with the hydrogen geocorona, and precipitative losses to the upper atmosphere, all considering full pitch angle distributions. The five independent variables that constitute the equatorial phase-space distribution function $F(t, \mathbf{r}_0, \mathbf{v}_0)$ are t, R_0, ϕ_0, W and $\mu_0 = cos(\alpha_0)$, where R_0 represents the radial distance on the magnetic equatorial surface (defined by the location of magnetic field minima (Ilie et al., 2012)), ϕ_0 is the equatorial Magnetic Local Time (MLT), W denotes the kinetic energy, and $\mu_0 = cos(\alpha_0)$ represents the cosine of the equatorial pitch angle of each species. The sizes of the numerical grids were carefully determined to resolve the features of interest, maintain numerical stability and accuracy, but also to optimize the run-time of the simulation. The grid used in each mutually independent phase-space variable is as follows: $20s$ time step; 20 equally spaced radial grid points distributed from $1.75R_E$ to $6.5R_E$ geocentric distance; 24 equally spaced points in local time around the Earth; 42 geometrically spaced energy cells from $10eV$ to $400keV$; and 71 pitch angle grid points from 90° to 0° (0 to 1 in μ_0). Because the kinetic equation is linear in this form, each hot plasma species can be considered individually and the total ring current bulk quantities, such as the equatorial pressure and current density, are obtained as the sums over all participating species. In addition, to calculate the bounce-averaged coefficients, HEIDI traces each individual field line whose equatorial intersection lies in the computation domain, and employs a field-aligned grid that discretizes each field line (starting and ending at the Earth's surface at certain magnetic foot points) uniformly or nonuniformly (set to 101 points along the field line for this study), along which the numerical integration is performed (Ilie et al., 2012). The source term on the right hand side of Equation 1 is represented by the plasma sheet conditions on the nightside outer boundary of the simulation domain, using plasma sheet particle fluxes as the outer boundary condition.

The HEIDI model considers the loss of each individual ring current hot ion species due to the charge exchange reactions with the neutral geocoronal hydrogen atom, which is expressed as:

$$H^+_{hot} + H \rightarrow H^+_{cold} + H \tag{2}$$

$$He^+_{hot} + H \rightarrow H^+_{cold} + He \tag{3}$$

$$O^+_{hot} + H \rightarrow H^+_{cold} + O \tag{4}$$

$$N^+_{hot} + H \rightarrow H^+_{cold} + N \tag{5}$$

where the H^+_{cold} on the right hand sides denotes the byproduct cold protons due to charge-exchange reactions with the corresponding energetic ring current ions. The effects of the

instantaneous charge exchange loss at simulation time t are reflected on the loss of equatorial distribution function $F_{X^+}(t, R_0, \phi_0, W, \mu_0)$ of all the energetic ring current ion species $X^+ \in \{H^+, He^+, O^+, N^+\}$ as:

$$F_{X^+(after)}(t, R_0, \phi_0, W, \mu_0) = F_{X^+(before)}(t, R_0, \phi_0, W, \mu_0) \cdot \eta_{X^+(CE)}(R_0, \phi_0, W, \mu_0) \quad (6)$$

where $F_{X^+(before)}(t, R_0, \phi_0, W, \mu_0)$ and $F_{X^+(after)}(t, R_0, \phi_0, W, \mu_0)$ represent the equatorial distribution function of ion X^+ before and after the charge exchange reactions, respectively. Furthermore, the term $\eta_{X^+(CE)}(R_0, \phi_0, W, \mu_0)$ in Equation 6 represents the local charge exchange loss factor of hot ion species $X^+ \in \{H^+, He^+, O^+, N^+\}$, calculated via:

$$\eta_{X^+(CE)}(R_0, \phi_0, W, \mu_0) = e^{-\sigma_{X^+}(W) v_{X^+}(W) \langle n_H \rangle (R_0, \phi_0, \mu_0) \Delta t} \quad (7)$$

where $\sigma_{X^+}(W)$ denotes the charge exchange cross section between the ring current hot ion species X^+ and the geocoronal neutral hydrogen (as a function of the kinetic energy W of the parent hot ion), $v_{X^+}(W)$ is the kinetic speed of the hot ion X^+ at energy W, Δt is the marching timestep, and $\langle n_H \rangle (R_0, \phi_0, \mu_0)$ is the equatorial bounce-averaged density of the geocoronal neutral hydrogen along the magnetic field line that intersects with the equatorial plane at (R_0, ϕ_0). Because the model currently only considers static hydrogen geocoronal models, the local charge exchange loss factor $\eta_{X^+(CE)}(R_0, \phi_0, W, \mu_0)$ is constant throughout the simulations due to the time independent geocoronal neutral hydrogen density distribution $\langle n_H \rangle (R_0, \phi_0, \mu_0)$.

With the transition from $F_{X^+(before)}$ to $F_{X^+(after)}$ under the effects of charge exchange loss as described in Equation 6, one is able to obtain the equatorial density distribution of the ring current species X^+ before and after the charge exchange loss, by evaluating the zeroth-order velocity moment of $F_{X^+(before)}$ and $F_{X^+(after)}$, respectively. We treated the lost density of ion species X^+ due to the charge exchange reaction to be the cold proton density resulting from X^+, considering the contribution from the parent energetic ions of all energies and equatorial pitch-angles, evaluated as:

$$\begin{aligned} n_{H^+_{cold}(X^+)}(t, R_0, \phi_0) &= n_{X^+(before)}(t, R_0, \phi_0) - n_{X^+(after)}(t, R_0, \phi_0) \\ &= \sum_k \sum_l F_{X^+(before)}(t, R_0, \phi_0, W_k, \mu_{0l})[1 - \eta_{X^+(CE)}(R_0, \phi_0, W_k, \mu_{0l})] W_k \mu_{0l} \end{aligned} \quad (8)$$

where k and l denote the discrete energy and equatorial pitch-angle indexes of the parent energetic ion species X^+, respectively. The total production of cold protons at each time step is accumulated, and the total cold byproduct proton density is obtained as the sum of the cold byproduct protons contributed by all the hot ion species, as shown in Equation 9. The cold protons are assumed to be neither interacting with each other, nor participating in Coulomb interactions with the hot ions.

$$n_{H^+_{cold}(total)} = n_{H^+_{cold}(H^+)} + n_{H^+_{cold}(He^+)} + n_{H^+_{cold}(O^+)} + n_{H^+_{cold}(N^+)} \quad (9)$$

3 Simulation Setup

Analysis of the density distribution of the cold protons produced via charge exchange illustrated in Equation 8 allows us to investigate the effects of hot plasma composition on the generation and evolution of the cold protons produced by charge-exchange reactions with the ring current ions. To make this assessment, we investigated the evolution of this cold proton distribution under different storm conditions and different plasma compositions, assuming idealized storm-like conditions and certain neutral hydrogen geocorona models, described below.

In this study, we consider two geocorona models: the spherically symmetric Rairden geocorona model (Rairden et al., 1986) and the Hodges geocorona model (Hodges, 1994), which allows for asymmetry in the neutral H density distribution both on the dawn-dusk, and day-night meridian. Panels (a) and (b) in Figure 1 show an example of the

bounce-averaged neutral hydrogen density (in log scale) as seen by energetic ions with an equatorial pitch-angle of 60° as predicted by Rairden et al. (1986) model and Hodges (1994) model. The neutral hydrogen density predicted by both geocorona models decreases exponentially toward larger L-shells, and while the Rairden et al. (1986) model possesses spherically symmetric nature, the Hodges (1994) model does not. Panel (c) in Figure 1 shows the percentage difference between the neutral densities predicted by the two models, indicating that the bounce-averaged neutral density predicted by the Hodges (1994) model is notably greater than that of the Rairden et al. (1986) model, with a significant intensification over the nightside.

The probability of charge exchange reactions of ring current ions with geocoronal neutral hydrogen also depends on the energy of the incident energetic particles and therefore, is determined by the charge exchange cross section. The HEIDI model adopts a recommended set of parametrized charge exchange cross sections given by Lindsay and Stebbings (2005), and the energy profile of the charge exchange cross section area (in log scale) is shown in panel (d) of Figure 1. Please note that the charge exchange cross sections of both N^+ (the black curve) and O^+ (the blue curve) with the cold neutral hydrogen are notably higher than that of energetic H^+ (the green curve) at a given ion energy, especially at higher energies. In addition, there are differences between the charge exchange cross section for energetic N^+ and neutral H reactions, vs. O^+ with neutral H over the entire energy range, which can be the reason for the different productions of charge-exchange byproduct cold H^+ from N^+ and O^+ illustrated in Section 4.1. Furthermore, there are large differences between the charge exchange cross section of energetic H^+ with neutral H reactions as the energy of the parent ion is increasing, implying that the probability of low energy H^+ undergoing charge exchange with geocoronal neutral hydrogen will be significantly greater than that for higher energy H^+ given the same local neutral density.

Numerical simulations are performed using an idealized 3-phase storm that lasts for 72 hours, with a quiet phase (the first 24 hours), a main phase (the middle 24 hours), and a recovery phase (the last 24 hours). The dipolar magnetic field is strictly imposed across the simulation domain throughout the entire storm. The source of the energetic ions is provided by the Kp-dependent nightside boundary ion flux updated every $120s$. The electric field is setup by the Kp-driven Volland-Stern's convection electric field model (Volland, 1973; Stern, 1975), which is a uniform dawn-dusk convection electric potential distribution applied across the simulation domain. The gradient of the electric potential depends on the Kp index, incurring a stronger Sunward $\vec{E}\times\vec{B}$ convection on local plasma during simulation times when Kp is higher.

The three different phases of the idealized geomagnetic storm are distinguished by the different Kp indices and nightside injection boundary conditions, as illustrated in panel (a) in both Figure 2 and Figure 3. During both the quiet phase and the recovery phase, the Kp was set to 1 and the total boundary injection ions density was set to $n_i = 2\ cm^{-3}$, which becomes 6 and 6 cm^{-3} during the main phase, respectively. The simulation transits from the quiet phase into the main phase in 3 hours from $T = 24h$ to $T = 27h$, during which both the Kp index and the total plasma sheet density n_i on the outer boundary increase linearly to the main phase value, and transits from the main phase into the recovery phase in 3 hours from $T = 51h$ to $T = 54h$, during which the Kp index and total ion plasma sheet density n_i on the outer boundary drop linearly to the quiet phase values. The ring current ion composition is set up by splitting the total ion plasma sheet ion density n_i on the outer boundary into H^+, He^+ and heavy ions (O^+ + N^+), via the Kp- and Ap-dependent statistical relationships derived by Young et al. (1982), which are based on previous geosynchronous orbit measurements (Liemohn et al., 1999). The composition of energetic heavy ions can be directly specified before the start of the simulation. In this study, we performed the 3-phase idealized storm simulation under two independent cases of heavy ions composition: one where all heavy ions are assumed to be

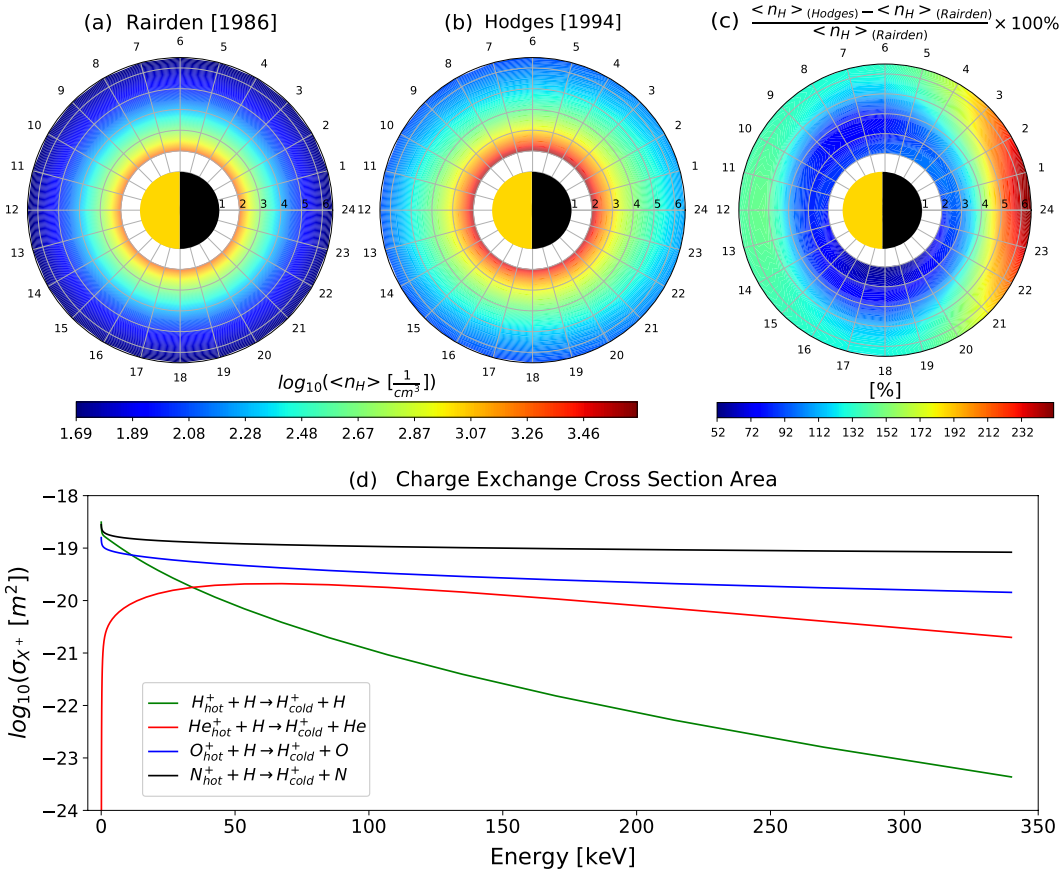

Figure 1. (a) and (b) Bounce-averaged neutral hydrogen density (on log scale) as seen by energetic ions with an equatorial pitch-angle of 60° as predicted by Rairden et al. (1986) model and Hodges (1994) model; (c) Percentage difference of the bounce-averaged geocoronal neutral density between the two models; (d) Energy profile of the cross section area of the charge exchange reactions between energetic ions X^+ and the geocoronal neutral hydrogen obtained from Lindsay and Stebbings (2005) and applied by the HEIDI model.

O^+, and the other where all heavy ions are assumed to be N^+. The simulation results are discussed in Section 4.

4 Results and Discussion

The simulation results are presented and discussed in this section, which is divided into three parts. Section 4.1 explores the formation and evolution of the charge-exchange byproduct cold protons from the energetic heavy ions, with a primary focus on the storm phase and recovery phase; Section 4.2 investigates the percentage contribution of the byproduct cold protons from the energetic heavy ions, and discusses the contribution structure of the heavy ions using different neutral geocorona models; Section 4.3 compares the density of the byproduct cold protons via charge exchange with an activity dependent plasmasphere model, and discusses the potential effects of the byproduct cold protons on the dynamics of the plasmasphere.

4.1 Cold H^+ Formed By Charge Exchange

Energetic heavy ions play a critical role in the production of the charge-exchange byproduct cold H^+ as they convect into the dipolar magnetosphere from the near-Earth portion of the magnetotail. We first examine the production of cold H^+ that resulted from the charge exchange of O^+ and N^+ ions with geocorona neutral H using the Rairden et al. (1986) geocorona model, and assuming that the heavy ions are either 100% O^+ or 100% N^+, respectively. While unrealistic, these assumptions are designed to illustrate the role of inner magnetospheric heavy ion composition in the production of cold H^+. Figure 2 shows the comparison between the ring current heavy ions densities and the associated cold H^+ as a charge-exchange byproduct at four times ($T_1 = 27h$, $T_2 = 40h$, $T_3 = 51h$ and $T_4 = 72h$) indicated at the top of row (b), as one reads from left to right. Each row shows the density of heavy ion (either O^+ or N^+) or the associated cold protons, as indicated by the highlighted red text at the bottom of each row.

At the beginning of the main phase ($T_1 = 27h$, the leftmost column), when both the convection strength and the particle flux on the nightside outer boundary are enhanced, we observe an increase in both O^+ and N^+ hot ion densities on the nightside centered on L=5 shell (as showed in the leftmost column of rows (b) and (d)), as injected particles are drifting westward and convecting into the lower L-shells. The leftmost column of rows (c) and (e) show that, by comparison with the ring current ion densities, there is no significant production of cold protons during the quiet phase, which implies that the effects of charge-exchange reactions are weak during this time. This is due to the relatively low ring current ion densities, as well as to the fact that the peak density occurs at higher L-shells where the geocoronal neutral density is low. During the main phase ($T_2 = 40h$, the second column from the left), we observe an enhancement in O^+ and N^+ densities in the evening sector (18MLT — 0MLT quadrant) between L = 3 and L = 5 shells, mostly due to the continuous supply of particles from the nightside boundary and strong Sunward convection strength, as showed in the second column from the left of rows (b) and (d). The second column from the left of rows (c) and (e) shows accumulation of the cold protons close to the model inner boundary across the duskside around L = 2.5 shell. This is due to the fact that the neutral density is exponentially decreasing with distance away from the Earth, therefore the charge exchange reaction is most effective at low radial distances. In addition, the cold protons generated at higher L-shells (closer to the peak of ring current) are also drifting westward while convecting Earthward, leading to an accumulation of cold protons at low L-shells. At the beginning of the recovery phase ($T_3 = 51h$, the third column from the left), the topology of the ring current becomes more symmetric. As energetic O^+ and N^+ drift around the simulation domain, they continue to undergo charge exchange reactions with the local geocoronal neutral hydrogen, especially at lower L-shells where the density of neutral hydrogen is high. Therefore, we observe a faster accumulation of cold protons accompanied with a faster decay of both O^+ and N^+ density at low L-shells. At the end of the simulation ($T_4 = 72h$, the fourth column from the left), the charge exchange losses led to a significant decay of energetic O^+ and N^+ densities as showed in the fourth column from the left of rows (b) and (d). This decay is associated with a significant accumulation of cold protons within L=4, as can be seen from the fourth column from the left of rows (c) and (e). The evolution of the cold H^+ population associated with energetic O^+ and N^+ over the four time instances illustrated above suggests that, the production and topology of the cold ion population are closely controlled by the conditions of ion plasma sheet along with the magnetospheric convection. The ion plasma sheet provides energetic ion populations that can be converted into the cold populations via charge exchange reactions, and the magnetospheric convection further accelerates the hot ion populations and drives them into lower L-shells where the geocorona neutral density is significantly higher. Therefore, it is the collective and accumulative effect of both ion plasma sheet composition and magnetospheric convection that determines the abundance and topology of the cold populations associated with the ring current energetic ions.

Although energetic ring current O^+ and N^+ possess similar qualitative behaviors across the four time instances as one compares row (b) with row (d), significant quantitative difference exists: the energetic N^+ decays notably faster than O^+ during the recovery phase, as reflected by the density of O^+ and N^+ showed in the fourth column from the left ($T_4 = 72h$) of rows (b) and (d), respectively. Part of the total loss of O^+ and N^+ during the recovery phase becomes the associated cold protons, therefore, observing that the density of cold protons associated with N^+ is notably higher than the one associated with O^+ (as one compares the fourth column from the left of row (e) with row (c)) implies that the ring current N^+ undergoes more efficient charge-exchange loss than O^+ does. We may attribute such a difference on the hot ions loss and cold H^+ production between O^+ and N^+ primarily to the difference of charge exchange cross section. The cross section of hot N^+ is always higher than that of O^+ across the entire considered energy range, inferring that the probability of energetic N^+ undergoing charge exchange reactions with the local cold neutral hydrogen is greater than that of energetic O^+, given the same local density of cold neutral hydrogen. As a result, energetic N^+ can be more efficient on producing cold protons, and therefore have a shorter average lifetime than energetic O^+.

4.2 Contribution of Cold H^+ By Energetic Heavy Ions

Next, we perform a quantitative analysis on how much energetic O^+ and N^+ contribute to the local production of cold H^+ generated by the charge exchange of ring current ions with neutral geocorona. Figure 3 shows the fraction of $\frac{H^+_{cold(heavy\ ions)}}{H^+_{cold(total)}}$ (expressed in percentage) at the same four time moments. The black contour lines represent different levels of the fraction $\frac{H^+_{cold(heavy\ ions)}}{H^+_{cold(total)}}$, where $H^+_{cold(heavy\ ions)}$ denotes the cold protons derived from the charge exchange process involving a particular ring current heavy ion species (either O^+ or N^+) as indicated under the label of each row, along with the background neutral geocorona model. These simulation results show that the contribution of cold protons associated with energetic O^+ via charge exchange reactions to the total cold proton population increases with decreasing distance from the Earth, with the 50% contribution contour at around L=4 shell for the simulation based on the Rairden et al. (1986) geocorona model (the fourth column from the left of row (b)). For the analogous simulation for which the geocorona density is provided by the Hodges (1994) model, the 50% contribution contour extends outward to L=5 shell (the fourth column from the left of row (c)). This implies that energetic O^+ ions are more likely to be convecting into lower L-shells before being lost via charge exchange, and consequently participate in additional charge-exchange reactions as they convect Earthward. On the other hand, the contribution of the cold protons associated with energetic N^+ to the total cold protons increases with increasing distance from the Earth, at both $T_3 = 51h$ and $T_4 = 72h$, as can be seen in both the third and the fourth columns from the left of rows (d) and (e). This is due to the fact that energetic N^+ is being lost in the charge exchange reaction significantly faster, therefore is less prone to convect deeper into the inner magnetosphere.

Furthermore, the production of cold H^+ is primarily determined by the plasma sheet composition, rather the neutral geocorona model. Numerical simulation results show that the increase in the neutral H density from the Rairden et al. (1986) to the Hodges (1994) model enhanced the charge-exchange reactions between energetic O^+ and neutral H, extending the 50% cold H^+ contribution contour from L=4 to L=5 shell at the end of the recovery phase; this is due to the fact that energetic O^+ ions are more likely to be convecting into lower L-shells where neutral H densityis larger. On the other hand, the region enclosed by the 60% contribution contour from energetic N^+ was reduced at the end of the recovery phase, as one can see in the fourth column from the left in row (d) to (e). The change of geocorona neutral model does not significantly affect the average contri-

bution rate of cold H^+ from both energetic O^+ and N^+ over the simulation domain: At the end of the recovery phase ($T_4 = 72h$), the average contribution of cold H^+ from energetic O^+ increases from 47.7% to 49.2%, with the peak value increases from 56.9% to 57.4%, as the geocorona model changes from the Rairden et al. (1986) to the Hodges (1994) model; on the other hand, the one from energetic N^+ decreases from 57.6% to 56.6%, with the peak value decreases from 66.1% to 61.4%. Therefore, the density of neutral H as predicted by various geocorona models is playing a less important role in shaping the peak and topology of the cold H^+ density, as compared with the plasma sheet heavy ion composition.

4.3 Effects of cold H^+ Formed By Charge Exchange on the Plasmasphere

Due to the spatial overlap between the plasmasphere and the ring current, the generation of cold H^+ via charge exchange can affect the dynamics of the plasmasphere. To investigate the effects of cold H^+ populations formed by charge exchange reactions on the plasmasphere, we adopted the activity-dependent Dynamic Global Core Plasma Model (DGCPM) (Ober et al., 1997) that provides the evolution of the equatorial thermal plasma density. The model tracks the advection of the magnetic flux tubes affected by the convection electric field and electric potential, which are directly controlled by the Kp index in the simulation, and solves the mass continuity equation along each moving field line for the total cold ion content. The plasmaspheric thermal plasma density distribution (in log scale) at four different time moments ($T_0 = 24h$, $T_3 = 51h$, $T_3^{'} = 58h$ and $T_4 = 72h$) are showed in row (b) of Figure 4. At the end of the quiet phase ($T_0 = 24h$, the leftmost column), the plasmaspheric cold density is approximately symmetric around the Earth with a slight dusk bulge. At the end of the storm phase ($T_3 = 51h$, the second column from the left), the plasmasphere has been significantly eroded, with the plasmaspheric drainage plume extending from the afternoon sector (18MLT — 0MLT quadrant) and a density trough has been formed on the nightside. The plasmasphere gradually refills during the recovery phase ($51h < T < 72h$), with the drainage plume rotating eastward and the thermal plasma density recovers. Therefore, the plasmasphere is highly dependent on the magnetospheric activity, as reflected by the dynamics of the shape of the plasmapause approximated by the boundary of the color maps in row (b). The cold H^+ population that resulted from the charge-exchange reactions contributes to the plasmaspheric thermal plasma density, therefore further affects the dynamics of the plasmasphere. Rows (c) and (e) of Figure 4 compares the shape of the plasmasphere considering (solid contours) and without considering (dashed contours) the contribution of the charge-exchange byproduct cold H^+ by energetic heavy ions (O^+ and N^+, respectively), showing that the byproduct cold H^+ resulting from energetic O^+ extends the plasmasphere boundary at dawn from L=2.75 to L=4, and those resulting from energetic N^+ extends it to L=4.25, at the beginning of the recovery phase ($T_3 = 51h$, the second column from the left of rows (c) and (e), red solid contour vs. red dashed contour). After 7 hours into the recovery phase, the cold H^+ that resulted from charge exchange reactions involving energetic O^+ extends the plasmasphere boundary at dawn from L=3.25 to L=4, and those resulting from charge exchange reactions involving energetic N^+ further extends it to L=4.5 ($T_3^{'} = 58h$, the third column from the left of rows (c) and (e), red solid contour vs. red dashed contour). Such an extension of the boundary of the plasmasphere during the early recovery phase due to the inclusion of cold H^+ produced via charge exchange reactions of neutral hydrogen with energetic heavy ions incurs significant expansion of the equatorial area of the plasmasphere, implying that the energetic heavy ions alone are able to produce cold protons in amounts significant enough to reshape the density distribution of the plasmasphere along with the plasmapause, especially in the early stage of the recovery phase. Furthermore, the cold H^+ that resulted from the total ring current ion species with different heavy ion compositions extends the plasmasphere with different extents, as one compares row (d) with (f). This implies that

the composition of the energetic heavy ions of the plasma sheet can affects the overall spatial extent of the plasmasphere.

The significant expansion of the plasmasphere boundary during the recovery phase suggests that the local density of cold H^+ produced via charge exchange with the ring current population can be abundant compared with the local plasmasphere density just beyond the plasmasphere boundary identified by the red dashed contours in Figure 4. Such local abundance of the cold H^+ can supply a significant amount to the plasmaspheric cold populations, therefore facilitating the local recovery rate. Figure 5 shows the ratio (in log scale) between the cold H^+ density and the plasmaspheric thermal plasma density provided by Ober et al. (1997) model, revealing a broad region of high density ratio (deep red) that lies on the nightside between L=3 to 5 and MLT=20 to 7 at the beginning of the recovery phase ($T_3 = 51h$, the second column from the left), which shrinks as the plasmasphere recovers. Comparing the location of the 10^1 cm^{-3} contour between the end of the quiet phase ($T_0 = 24h$) and the start of the recovery phase ($T_3 = 51h$), one can identify a plasmasphere density trough in which the plasmaspheric cold plasma population is significantly eroded during the storm phase, and the most of the high-ratio region, including the global ratio peak, is overlapping with the trough. Furthermore, the local production of cold H^+ by total ring current ion species (row (d)) can be at most 13.6 times the local plasmasphere cold density as predicted by the DGCPM model, assuming all the heavy ions are N^+, with the ones by energetic N^+ (row (c)) be at most 8.5, after 7 hours into the recovery phase ($T_3^{'} = 58h$). In the case when all the energetic heavy ions are O^+, the local production of cold H^+ by total ring current ions (row (b)) can be at most 10 times the original local plasmasphere cold density, and the ones by energetic O^+ (row (a)) be at most $\sim$5 times, at $T_3^{'} = 58h$. Therefore, the charge-exchange produced cold protons can notably enhance the local plasmaspheric refilling rate, especially in the density trough during the early stage of the recovery phase.

5 Summary and Conclusion

In this study, we assessed the role of plasma sheet ion composition and geocorona neutral H models in the production and transport of cold protons as byproduct of charge exchange reactions with the ring current population. The simulation results show that: (1) the production and topology of the cold H^+ population produced via charge-exchange reactions with ring current ions are closely controlled by the composition of plasma sheet and the magnetospheric convection; (2) the geocorona neutral density distribution does not play a significant role in shaping the peak density and overall topology of the byproduct cold proton structure, which is instead shown to be primarily determined by the composition of energetic heavy ions (O^+ and N^+); (3) the charge-exchange byproduct cold protons can reshape the density distribution of the plasmasphere along with the plasmapause, and have the potential to enhance the early-stage plasmaspheric refilling rate by supplying to the plasmasphere density trough; (4) the cold protons deriving from charge exchange reactions of energetic O^+ with neutral H populate the inner L shells, while the cold protons deriving from charge exchange reactions of energetic N^+ with neutral H populate the larger L-shells.

Numerical simulations are performed under the assumption that the heavy ions are either 100% O^+ or 100% N^+. Albeit idealized, these numerical experiments reveal potential aspects with profound impacts on the generation and evolution of the cold populations, including the plasma sheet condition, magnetospheric convection, and composition of energetic heavy ions. It is also inferred that the generation of cold H^+ as a byproduct of charge exchange can affect the local refilling of the plasmasphere during the early recovery phase.

Open Research

The HEIDI model has been included in the Space Weather Modeling Framework (SWMF), which is available for download at http://csem.engin.umich.edu/tools/swmf. The full set of simulation data is available at https://doi.org/10.6084/m9.figshare.c.5979331.v1.

Acknowledgments

Work at University of Illinois at Urbana-Champaign was performed with financial support from the NASA grant N99066ZO, NASA grant 80NSSC20K1231, the NSF award 1664078 and NSF CAREER award 1945573. Work at University of Michigan was performed with financial support from the NASA grants 80NSSC19K0077 and 80NSSC17K0015. Joseph E. Borovsky was supported by the NSF GEM Program via grant AGS-2027569.

References

Andersson, L., Peterson, W. K., & McBryde, K. M. (2004). Dynamic coordinates for auroral ion outflow. *Journal of Geophysical Research: Space Physics*, *109*(A8). Retrieved from `https://agupubs.onlinelibrary.wiley.com/doi/abs/10.1029/2004JA010424` doi: https://doi.org/10.1029/2004JA010424

Artemyev, A. V., Angelopoulos, V., Runov, A., & Zhang, X.-J. (2020). Ionospheric outflow during the substorm growth phase: Themis observations of oxygen ions at the plasma sheet boundary. *Journal of Geophysical Research: Space Physics*, *125*(7), e2019JA027612. Retrieved from `https://agupubs.onlinelibrary.wiley.com/doi/abs/10.1029/2019JA027612` (e2019JA027612 10.1029/2019JA027612) doi: https://doi.org/10.1029/2019JA027612

Borovsky, J. E., Denton, M. H., Denton, R. E., Jordanova, V. K., & Krall, J. (2013). Estimating the effects of ionospheric plasma on solar wind/magnetosphere coupling via mass loading of dayside reconnection: Ion-plasma-sheet oxygen, plasmaspheric drainage plumes, and the plasma cloak. *Journal of Geophysical Research: Space Physics*, *118*(9), 5695-5719. Retrieved from `https://agupubs.onlinelibrary.wiley.com/doi/abs/10.1002/jgra.50527` doi: https://doi.org/10.1002/jgra.50527

Borovsky, J. E., Liu, J., Ilie, R., & Liemohn, M. W. (2022). Charge-exchange byproduct cold protons in the earth's magnetosphere. *Frontiers in Astronomy and Space Sciences*, *8*. Retrieved from `https://www.frontiersin.org/article/10.3389/fspas.2021.785305` doi: 10.3389/fspas.2021.785305

Brambles, O. J., Lotko, W., Damiano, P. A., Zhang, B., Wiltberger, M., & Lyon, J. (2010). Effects of causally driven cusp o+ outflow on the storm time magnetosphere-ionosphere system using a multifluid global simulation. *Journal of Geophysical Research: Space Physics*, *115*(A9). Retrieved from `https://agupubs.onlinelibrary.wiley.com/doi/abs/10.1029/2010JA015469` doi: https://doi.org/10.1029/2010JA015469

Brambles, O. J., Lotko, W., Zhang, B., Wiltberger, M., Lyon, J., & Strangeway, R. J. (2011, jun). Magnetosphere sawtooth oscillations induced by ionospheric outflow. *Science (New York, N.Y.)*, *332*(6034), 1183–6. doi: 10.1126/science.1202869

Carruthers, G. R., Page, T., & Meier, R. R. (1976, April). Apollo 16 Lyman alpha imagery of the hydrogen geocorona. *Journal of Geophysical Research: Space Physics*, *81*, 1664-1672. doi: 10.1029/JA081i010p01664

Chamberlain, J. W. (1963, August). Planetary coronae and atmospheric evaporation. *Planet. Space Sci.*, *11*, 901-+. doi: 10.1016/0032-0633(63)90122-3

Chappell, C. R., Moore, T. E., & Waite Jr., J. H. (1987). The ionosphere as a fully adequate source of plasma for the Earth's magnetosphere. *Journal of Geophysical Research: Space Physics*, *92*(A6), 5896-5910. Retrieved from `https://`

agupubs.onlinelibrary.wiley.com/doi/abs/10.1029/JA092iA06p05896 doi: 10.1029/JA092iA06p05896

Coley, W. R., Heelis, R. A., & Hairston, M. R. (2003, December). High-latitude plasma outflow as measured by the DMSP spacecraft. *Journal of Geophysical Research*, *108*(A), 1441.

Cornwall, J. M. (1977). On the role of charge exchange in generating unstable waves in the ring current. *Journal of Geophysical Research (1896-1977)*, *82*(7), 1188-1196. Retrieved from https://agupubs.onlinelibrary.wiley.com/doi/abs/10.1029/JA082i007p01188 doi: https://doi.org/10.1029/JA082i007p01188

Dandouras, I. (2021). Ion outflow and escape in the terrestrial magnetosphere: Cluster advances. *Journal of Geophysical Research: Space Physics*, *126*(10), e2021JA029753. Retrieved from https://agupubs.onlinelibrary.wiley.com/doi/abs/10.1029/2021JA029753 (e2021JA029753 2021JA029753) doi: https://doi.org/10.1029/2021JA029753

Delzanno, G. L., Borovsky, J. E., Henderson, M. G., Resendiz Lira, P. A., Royter-shteyn, V., & Welling, D. T. (2021). The impact of cold electrons and cold ions in magnetospheric physics. *Journal of Atmospheric and Solar-Terrestrial Physics*, *220*, 105599. Retrieved from https://www.sciencedirect.com/science/article/pii/S1364682621000596 doi: https://doi.org/10.1016/j.jastp.2021.105599

Denton, M., & Borovsky, J. (2014, 11). Observations and modeling of magnetic flux tube refilling of the plasmasphere at geosynchronous orbit. *Journal of Geophysical Research: Space Physics*, *119*. doi: 10.1002/2014JA020491

Denton, M. H., Reeves, G. D., Thomsen, M. F., Henderson, M. G., Friedel, R. H. W., Larsen, B., ... Kletzing, C. A. (2016). The complex nature of storm-time ion dynamics: Transport and local acceleration. *Geophysical Research Letters*, *43*(19), 10,059–10,067. Retrieved from http://dx.doi.org/10.1002/2016GL070878 (2016GL070878) doi: 10.1002/2016GL070878

Denton, M. H., Thomsen, M. F., Korth, H., Lynch, S., Zhang, J. C., & Liemohn, M. W. (2005, July). Bulk plasma properties at geosynchronous orbit. *Journal of Geophysical Research (Space Physics)*, *110*(A9), 7223-+. doi: 10.1029/2004JA010861

Dessler, A. J., Hanson, W. B., & Parker, E. N. (1961). Formation of the geomagnetic storm main-phase ring current. *Journal of Geophysical Research (1896-1977)*, *66*(11), 3631-3637. Retrieved from https://agupubs.onlinelibrary.wiley.com/doi/abs/10.1029/JZ066i011p03631 doi: https://doi.org/10.1029/JZ066i011p03631

Fu, S. Y., Wilken, B., Zong, Q. G., & Pu, Z. Y. (2001). Ion composition variations in the inner magnetosphere: Individual and collective storm effects in 1991. *Journal of Geophysical Research: Space Physics*, *106*(A12), 29683-29704. Retrieved from https://agupubs.onlinelibrary.wiley.com/doi/abs/10.1029/2000JA900173 doi: https://doi.org/10.1029/2000JA900173

Genestreti, K. J., Goldstein, J., Corley, G. D., Farner, W., Kistler, L. M., Larsen, B. A., ... Turner, N. E. (2017). Temperature of the plasmasphere from van allen probes hope. *Journal of Geophysical Research: Space Physics*, *122*(1), 310-323. Retrieved from https://agupubs.onlinelibrary.wiley.com/doi/abs/10.1002/2016JA023047 doi: https://doi.org/10.1002/2016JA023047

Gershman, D. J., Avanov, L. A., Boardsen, S. A., Dorelli, J. C., Gliese, U., Barrie, A. C., ... Pollock, C. J. (2017). Spacecraft and instrument photoelectrons measured by the dual electron spectrometers on mms. *Journal of Geophysical Research: Space Physics*, *122*(11), 11,548-11,558. Retrieved from https://agupubs.onlinelibrary.wiley.com/doi/abs/10.1002/2017JA024518 doi: https://doi.org/10.1002/2017JA024518

Glocer, A., Tóth, G., Gombosi, T., & Welling, D. (2009, May). Modeling ionospheric outflows and their impact on the magnetosphere, initial results. *Jour-*

nal of Geophysical Research (Space Physics), *114*(A13), 5216-+. doi: 10.1029/2009JA014053

Haaland, S., Eriksson, A., André, M., Maes, L., Baddeley, L., Barakat, A., ... Welling, D. (2015). Estimation of cold plasma outflow during geomagnetic storms. *Journal of Geophysical Research: Space Physics*, *120*(12), 10,622-10,639. Retrieved from https://agupubs.onlinelibrary.wiley.com/doi/abs/10.1002/2015JA021810 doi: https://doi.org/10.1002/2015JA021810

He, F., Zhang, X.-X., Wang, X.-Y., & Chen, B. (2015). Euv emissions from solar wind charge exchange in the earth's magnetosheath: Three-dimensional global hybrid simulation. *Journal of Geophysical Research: Space Physics*, *120*(1), 138-156. Retrieved from https://agupubs.onlinelibrary.wiley.com/doi/abs/10.1002/2014JA020521 doi: https://doi.org/10.1002/2014JA020521

Hodges, R. R., Jr. (1994, December). Monte Carlo simulation of the terrestrial hydrogen exosphere. *Journal of Geophysical Research: Space Physics*, *99*, 23229-+. doi: 10.1029/94JA02183

Huddleston, M. M., Chappell, C. R., Delcourt, D. C., Moore, T. E., Giles, B. L., & Chandler, M. O. (2005). An examination of the process and magnitude of ionospheric plasma supply to the magnetosphere. *Journal of Geophysical Research: Space Physics*, *110*(A12). Retrieved from https://agupubs.onlinelibrary.wiley.com/doi/abs/10.1029/2004JA010401 doi: https://doi.org/10.1029/2004JA010401

Hultqvist, B. (1979, June). The hot ion component of the magnetospheric plasma and some relations to the electron component - Observations and physical implications. *Space Science Reviews*, *23*(4), 581–675.

Hultqvist, B. (1982). Recent progress in the understanding of the ion composition in the magnetosphere and some major question marks. *Reviews of Geophysics*, *20*(3), 589-611. Retrieved from https://agupubs.onlinelibrary.wiley.com/doi/abs/10.1029/RG020i003p00589 doi: https://doi.org/10.1029/RG020i003p00589

Ilie, R., & Liemohn, M. W. (2016, September). The outflow of ionospheric nitrogen ions: A possible tracer for the altitude-dependent transport and energization processes of ionospheric plasma. *Journal of Geophysical Research: Space Physics*, *121*(9), 9250–9255.

Ilie, R., Liemohn, M. W., & Toth, G. (2015). Testing the magnetotail configuration based low 2 altitude isotropic boundaries. *Journal of Geophysical Research (Space Physics)*. (2015JA021858) doi: 10.1002/2015JA021858

Ilie, R., Liemohn, M. W., Toth, G., & Skoug, R. M. (2012). Kinetic model of the inner magnetosphere with arbitrary magnetic field. *Journal of Geophysical Research: Space Physics*, *117*(A4). Retrieved from https://agupubs.onlinelibrary.wiley.com/doi/abs/10.1029/2011JA017189 doi: 10.1029/2011JA017189

Ilie, R., Skoug, R., Funsten, H., Liemohn, M., Bailey, J., & Gruntman, M. (2013). The impact of geocoronal density on ring current development. *Journal of Atmospheric and Solar-Terrestrial Physics*, *99*, 92 - 103. Retrieved from http://www.sciencedirect.com/science/article/pii/S1364682612000946 (Dynamics of the Complex Geospace System) doi: https://doi.org/10.1016/j.jastp.2012.03.010

James, M. K., Yeoman, T. K., Jones, P., Sandhu, J. K., & Goldstein, J. (2021). The scalable plasma ion composition and electron density (spiced) model for earth's inner magnetosphere. *Journal of Geophysical Research: Space Physics*, *126*(9), e2021JA029565. Retrieved from https://agupubs.onlinelibrary.wiley.com/doi/abs/10.1029/2021JA029565 (e2021JA029565 2021JA029565) doi: https://doi.org/10.1029/2021JA029565

Keika, K., Nosé, M., Brandt, P. C., Ohtani, S., Mitchell, D. G., & Roelof, E. C. (2006, November). Contribution of charge exchange loss to the storm time ring

current decay: IMAGE/HENA observations. *Journal of Geophysical Research (Space Physics)*, *111*(A10), 11-+. doi: 10.1029/2006JA011789

Kistler, L. M., Ipavich, F. M., Hamilton, D. C., Gloeckler, G., Wilken, B., Kremser, G., & Stüdemann, W. (1989). Energy spectra of the major ion species in the ring current during geomagnetic storms. *Journal of Geophysical Research: Space Physics*, *94*(A4), 3579-3599. Retrieved from https://agupubs.onlinelibrary.wiley.com/doi/abs/10.1029/JA094iA04p03579 doi: 10.1029/JA094iA04p03579

Kistler, L. M., & Mouikis, C. G. (2016, March). The inner magnetosphere ion composition and local time distribution over a solar cycle. *Journal of Geophysical Research: Space Physics*, *121*(3), 2009–2032.

Kozyra, J. U., Liemohn, M. W., Clauer, C. R., Ridley, A. J., Thomsen, M. F., Borovsky, J. E., ... Gonzalez, W. D. (2002, August). Multistep Dst development and ring current composition changes during the 4-6 June 1991 magnetic storm. *Journal of Geophysical Research (Space Physics)*, *107*, 1224-+. doi: 10.1029/2001JA000023

Lawrence, D., Thomsen, M., Borovsky, J., & McComas, D. (1999). Measurements of early and late time plasmasphere refilling as observed from geosynchronous orbit. *Journal of Geophysical Research: Space Physics*, *104*(A7), 14691–14704. doi: 10.1029/1998ja900087

Lee, J. H., Blum, L. W., & Chen, L. (2021). On the impacts of ions of ionospheric origin and their composition on magnetospheric emic waves. *Frontiers in Astronomy and Space Sciences*, *8*, 122. Retrieved from https://www.frontiersin.org/article/10.3389/fspas.2021.719715 doi: 10.3389/fspas.2021.719715

Liemohn, M. W. (2006). Introduction to special section on "results of the national science foundation geospace environment modeling inner magnetosphere/storms assessment challenge". *Journal of Geophysical Research: Space Physics*, *111*(A11). Retrieved from https://agupubs.onlinelibrary.wiley.com/doi/abs/10.1029/2006JA011970 doi: https://doi.org/10.1029/2006JA011970

Liemohn, M. W., & Kozyra, J. U. (2003, May). Lognormal form of the ring current energy content. *Journal of Atmospheric and Solar-Terrestrial Physics*, *65*, 871-886. doi: 10.1016/S1364-6826(03)00088-9

Liemohn, M. W., & Kozyra, J. U. (2005). Testing the Hypothesis That Charge Exchange Can Cause a Two-Phase Decay. In T. I. Pulkkinen, N. A. Tsyganenko, & R. H. W. Friedel (Ed.), *The inner magnetosphere: Physics and modeling* (Vol. 155, p. 211-+).

Liemohn, M. W., Kozyra, J. U., Jordanova, V. K., Khazanov, G. V., Thomsen, M. F., & Cayton, T. E. (1999). Analysis of early phase ring current recovery mechanisms during geomagnetic storms. *Geophysical Research Letters*, *26*(18), 2845-2848. Retrieved from https://agupubs.onlinelibrary.wiley.com/doi/abs/10.1029/1999GL900611 doi: 10.1029/1999GL900611

Liemohn, M. W., Ridley, A. J., Gallagher, D. L., Ober, D. M., & Kozyra, J. U. (2004). Dependence of plasmaspheric morphology on the electric field description during the recovery phase of the 17 April 2002 magnetic storm. *Journal of Geophysical Research: Space Physics*, *109*(A3). Retrieved from https://agupubs.onlinelibrary.wiley.com/doi/abs/10.1029/2003JA010304 doi: 10.1029/2003JA010304

Lindsay, B. G., & Stebbings, R. F. (2005, December). Charge transfer cross sections for energetic neutral atom data analysis. *Journal of Geophysical Research (Space Physics)*, *110*(A9), 12213. doi: 10.1029/2005JA011298

Milillo, A., Orsini, S., Daglis, I. A., & Bellucci, G. (1996). Low-altitude energetic neutral atoms imaging of the inner magnetosphere: A geometrical method to identify the energetic neutral atoms contributions from different magneto-

spheric regions. *Journal of Geophysical Research: Space Physics*, *101*(A12), 27123-27131. Retrieved from https://agupubs.onlinelibrary.wiley.com/doi/abs/10.1029/96JA01560 doi: https://doi.org/10.1029/96JA01560

Moore, T. E., Chappell, C. R., Chandler, M. O., Craven, P. D., Giles, B. L., Pollock, C. J., ... Mozer, F. S. (1997). High-altitude observations of the polar wind. *Science*, *277*(5324), 349-351. Retrieved from https://www.science.org/doi/abs/10.1126/science.277.5324.349 doi: 10.1126/science.277.5324.349

Mozer, F., Agapitov, O., Angelopoulos, V., Hull, A., Larson, D., Lejosne, S., & McFadden, J. (2016, 12). Extremely field-aligned cool electrons in the dayside outer magnetosphere: Field-aligned cool electrons. *Geophysical Research Letters*, *44*. doi: 10.1002/2016GL072054

Obana, Y., Menk, F. W., & Yoshikawa, I. (2010). Plasma refilling rates for l = 2.3–3.8 flux tubes. *Journal of Geophysical Research: Space Physics*, *115*(A3). Retrieved from https://agupubs.onlinelibrary.wiley.com/doi/abs/10.1029/2009JA014191 doi: https://doi.org/10.1029/2009JA014191

Ober, D. M., Horwitz, J. L., & Gallagher, D. L. (1997, July). Formation of density troughs embedded in the outer plasmasphere by subauroral ion drift events. *Journal of Geophysical Research: Space Physics*, *102*, 14595-14602. doi: 10.1029/97JA01046

Orsini, S. (2004). Modeling the time-evolving plasma in the inner magnetosphere: An empirical approach. *Journal of Geophysical Research*, *109*(A11), 18,391.

Ouellette, J. E., Brambles, O. J., Lyon, J. G., Lotko, W., & Rogers, B. N. (2013). Properties of outflow-driven sawtooth substorms. *Journal of Geophysical Research: Space Physics*, *118*(6), 3223-3232. Retrieved from https://agupubs.onlinelibrary.wiley.com/doi/abs/10.1002/jgra.50309 doi: https://doi.org/10.1002/jgra.50309

Rairden, R. L., Frank, L. A., & Craven, J. D. (1986, December). Geocoronal imaging with Dynamics Explorer. *Journal of Geophysical Research: Space Physics*, *91*, 13613-13630. doi: 10.1029/JA091iA12p13613

Smith, P. H., & Bewtra, N. K. (1978, March). Charge exchange lifetimes for ring current ions. *Space Science Reviews*, *22*, 301-318. doi: 10.1007/BF00239804

Sojka, J. J., & Wrenn, G. L. (1985). Refilling of geosynchronous flux tubes as observed at the equator by geos 2. *Journal of Geophysical Research: Space Physics*, *90*(A7), 6379-6385. Retrieved from https://agupubs.onlinelibrary.wiley.com/doi/abs/10.1029/JA090iA07p06379 doi: https://doi.org/10.1029/JA090iA07p06379

Stern, D. P. (1975). The motion of a proton in the equatorial magnetosphere. *Journal of Geophysical Research (1896-1977)*, *80*(4), 595-599. Retrieved from https://agupubs.onlinelibrary.wiley.com/doi/abs/10.1029/JA080i004p00595 doi: 10.1029/JA080i004p00595

Su, Y.-J., Thomsen, M. F., Borovsky, J. E., & Lawrence, D. J. (2001). A comprehensive survey of plasmasphere refilling at geosynchronous orbit. *Journal of Geophysical Research: Space Physics*, *106*(A11), 25615-25629. Retrieved from https://agupubs.onlinelibrary.wiley.com/doi/abs/10.1029/2000JA000441 doi: https://doi.org/10.1029/2000JA000441

Thomsen, M. F., Denton, M. H., Gary, S. P., Liu, K., & Min, K. (2017, December). Ring/Shell Ion Distributions at Geosynchronous Orbit. *Journal of Geophysical Research: Space Physics*, *122*(1), 12–.

Thomsen, M. F., Denton, M. H., Jordanova, V. K., Chen, L., & Thorne, R. M. (2011). Free energy to drive equatorial magnetosonic wave instability at geosynchronous orbit. *Journal of Geophysical Research: Space Physics*, *116*(A8). Retrieved from https://agupubs.onlinelibrary.wiley.com/doi/abs/10.1029/2011JA016644 doi: https://doi.org/10.1029/2011JA016644

Trung, H.-S., Liemohn, M. W., & Ilie, R. (2019). Steady state characteristics of the terrestrial geopauses. *Journal of Geophysical Research: Space Physics*,

124(7), 5070-5081. Retrieved from https://agupubs.onlinelibrary.wiley.com/doi/abs/10.1029/2019JA026636 doi: https://doi.org/10.1029/2019JA026636

Volland, H. (1973). A semiempirical model of large-scale magnetospheric electric fields. *Journal of Geophysical Research (1896-1977)*, *78*(1), 171-180. Retrieved from https://agupubs.onlinelibrary.wiley.com/doi/abs/10.1029/JA078i001p00171 doi: 10.1029/JA078i001p00171

Welling, D. T., André, M., Dandouras, I., Delcourt, D., Fazakerley, A., Fontaine, D., ... Yau, A. (2015, oct). The Earth: Plasma Sources, Losses, and Transport Processes. *Space Science Reviews*, *192*(1-4), 145–208. Retrieved from http://link.springer.com/10.1007/s11214-015-0187-2 doi: 10.1007/s11214-015-0187-2

Welling, D. T., Jordanova, V. K., Glocer, A., Toth, G., Liemohn, M. W., & Weimer, D. R. (2015, jun). The two-way relationship between ionospheric outflow and the ring current. *Journal of Geophysical Research: Space Physics*, *120*(6), 4338–4353. Retrieved from http://doi.wiley.com/10.1002/2015JA021231 doi: 10.1002/2015JA021231

Welling, D. T., & Ridley, A. J. (2010, April). Exploring sources of magnetospheric plasma using multispecies MHD. *Journal of Geophysical Research*, *115*(A), A04201.

Wiltberger, M., Lotko, W., Lyon, J. G., Damiano, P., & Merkin, V. (2010, October). Influence of cusp O+ outflow on magnetotail dynamics in a multifluid MHD model of the magnetosphere. *Journal of Geophysical Research*, *115*(1), A00J05.

Winglee, R. M. (2000). Mapping of ionospheric outflows into the magnetosphere for varying IMF conditions. *Journal of Atmospheric and Solar-Terrestrial Physics*, *62*, 527–540. Retrieved from http://www.sciencedirect.com/science/article/pii/S1364682600000158

Winglee, R. M., Chua, D., Brittnacher, M., Parks, G. K., & Lu, G. (2002, September). Global impact of ionospheric outflows on the dynamics of the magnetosphere and cross-polar cap potential. *Journal of Geophysical Research (Space Physics)*, *107*, 1237. doi: 10.1029/2001JA000214

Young, D. T., Balsiger, H., & Geiss, J. (1982). Correlations of magnetospheric ion composition with geomagnetic and solar activity. *Journal of Geophysical Research: Space Physics*, *87*(A11), 9077-9096. Retrieved from https://agupubs.onlinelibrary.wiley.com/doi/abs/10.1029/JA087iA11p09077 doi: 10.1029/JA087iA11p09077

Yu, Y., Liemohn, M. W., Jordanova, V. K., Lemon, C., & Zhang, J. (2019). Recent advancements and remaining challenges associated with inner magnetosphere cross-energy/population interactions (imcepi). *Journal of Geophysical Research: Space Physics*, *124*(2), 886-897. Retrieved from https://agupubs.onlinelibrary.wiley.com/doi/abs/10.1029/2018JA026282 doi: https://doi.org/10.1029/2018JA026282

Zhao, H., Li, X., Baker, D. N., Fennell, J. F., Blake, J. B., Larsen, B. A., ... Rodriguez, J. V. (2015). The evolution of ring current ion energy density and energy content during geomagnetic storms based on Van Allen Probes measurements. *Journal of Geophysical Research: Space Physics*, *120*(9), 7493–7511. Retrieved from http://dx.doi.org/10.1002/2015JA021533 doi: 10.1002/2015JA021533

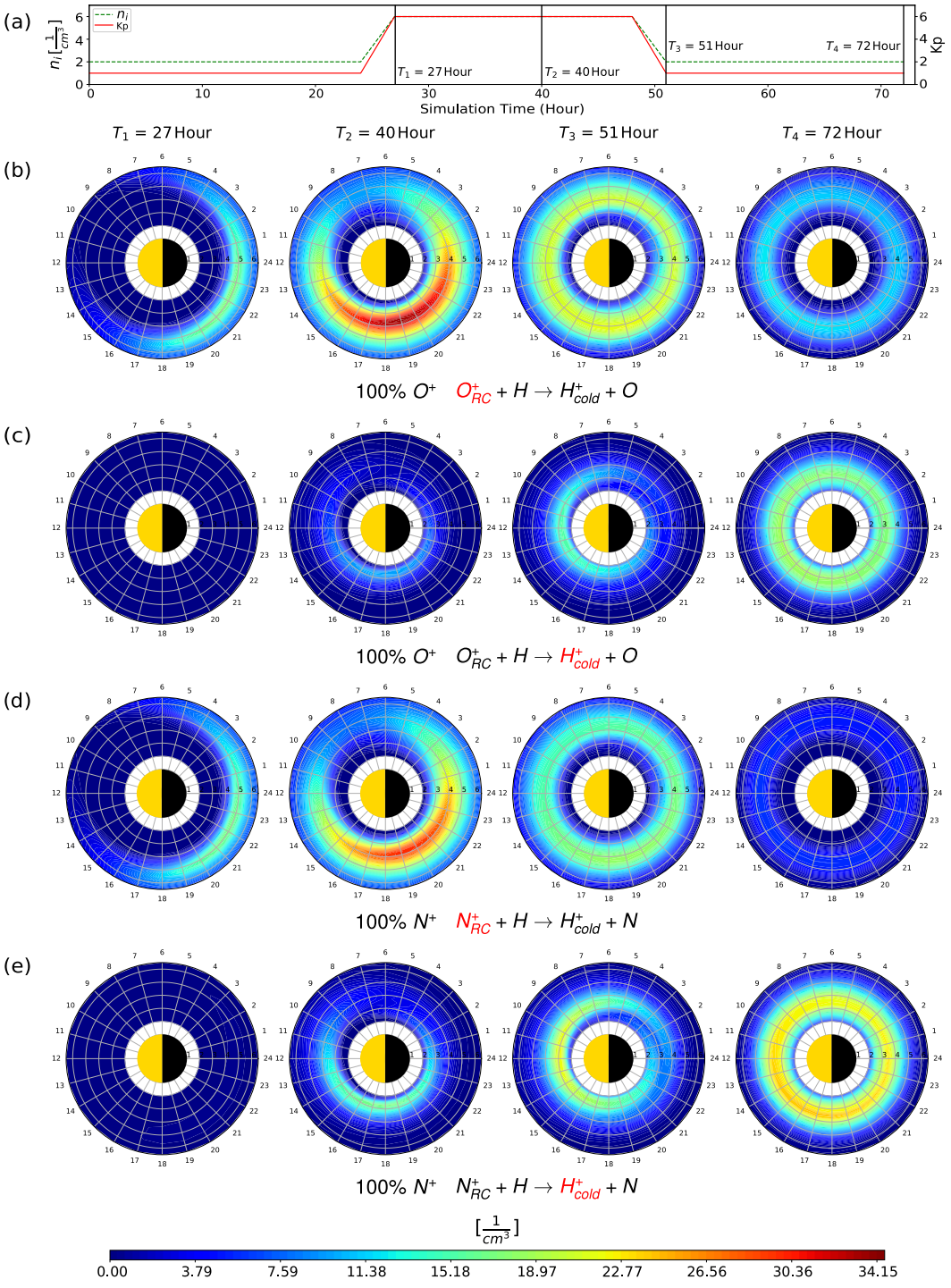

Figure 2. (a) Evolutionary tracks of the input parameters for the idealized storm simulations showing the Kp index (right y-axis, red line) and plasma sheet ion density on the nightside outer boundary (left y-axis, green line); (b) and (c) Evolution of ring current heavy ions density (100% O^+) and the associated charge-exchange byproduct cold protons by the energetic heavy ions at four time instances; (d) and (e) Evolution of ring current heavy ions density (100% N^+) and the associated charge-exchange byproduct cold protons by the energetic heavy ions at four time instances. The symmetric Rairden et al. (1986) model is used.

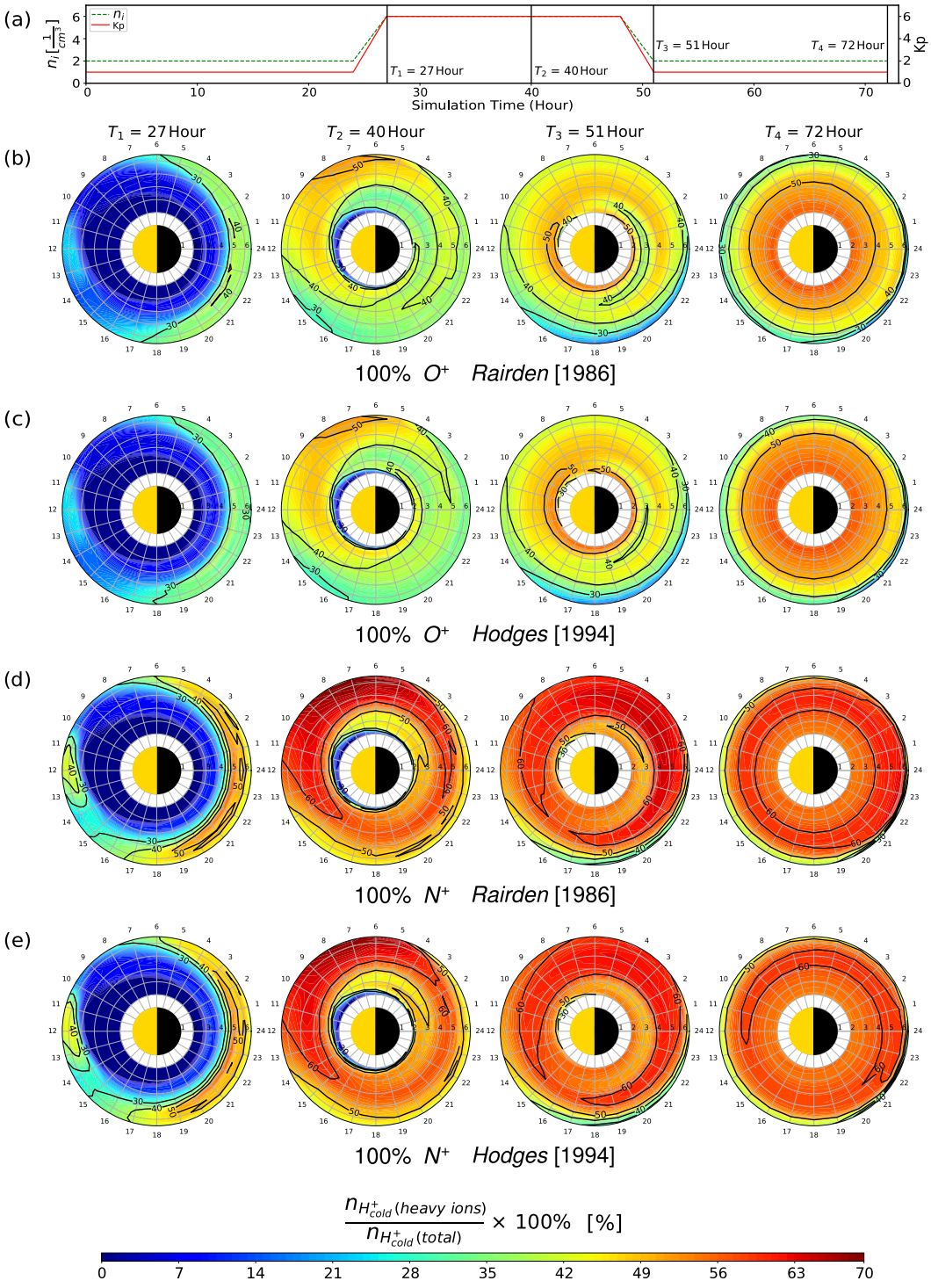

Figure 3. (a) Evolutionary tracks of the input parameters for the idealized storm simulations showing the Kp index (right y-axis, red line) and plasma sheet density on the nightside outer boundary (left y-axis, green line); (b) and (c) Evolution of the ratio (in %) between the local charge-exchange byproduct cold protons density produced by hot heavy ions (100% O^+) and the one produced by total energetic ring current ions, under Rairden et al. (1986) model and Hodges (1994) model; (d) and (e) Evolution of the ratio (in %) between the local charge-exchange byproduct cold protons density produced by hot heavy ions (100% N^+) and the one produced by total energetic ring current ions, under Rairden et al. (1986) model and Hodges (1994) model. Row (c) and row (e) assume the boundary injection heavy ions are 100% of O^+ and N^+, respectively, but under the Hodges geocoronal model.

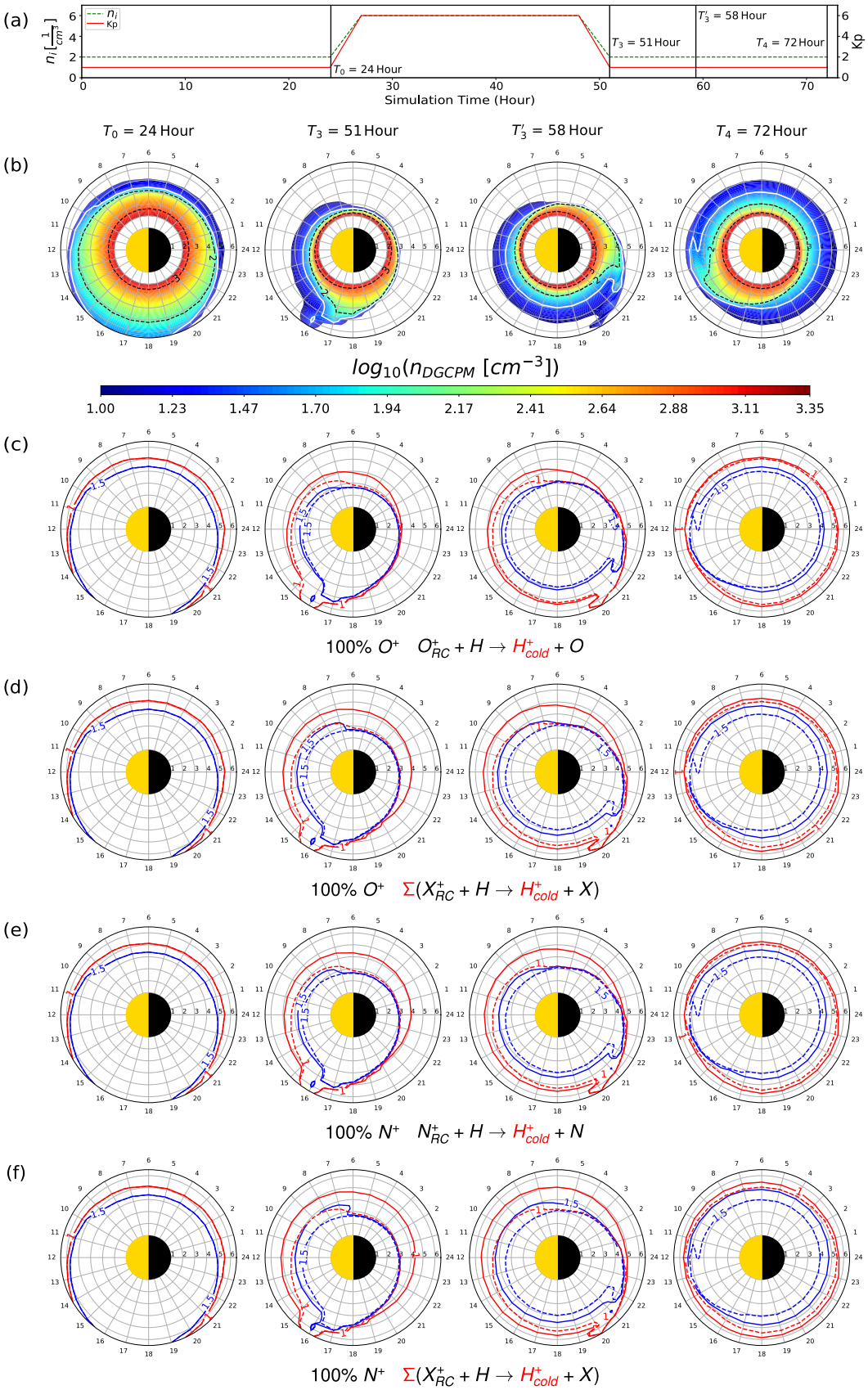

Figure 4. (a) Evolutionary tracks of the input parameters for the idealized storm simulations; (b) Evolution of equatorial plasmaspheric thermal plasma density predicted by Ober et al. (1997) plasmasphere model (in log scale), with the white solid contour marks at constant density level of 30 cm^{-3}; (c) to (f) Density contour levels (in log scale) of Ober et al. (1997) model (dashed) and the ones after considering the contribution from the charge-exchange byproduct cold H^+ popula-

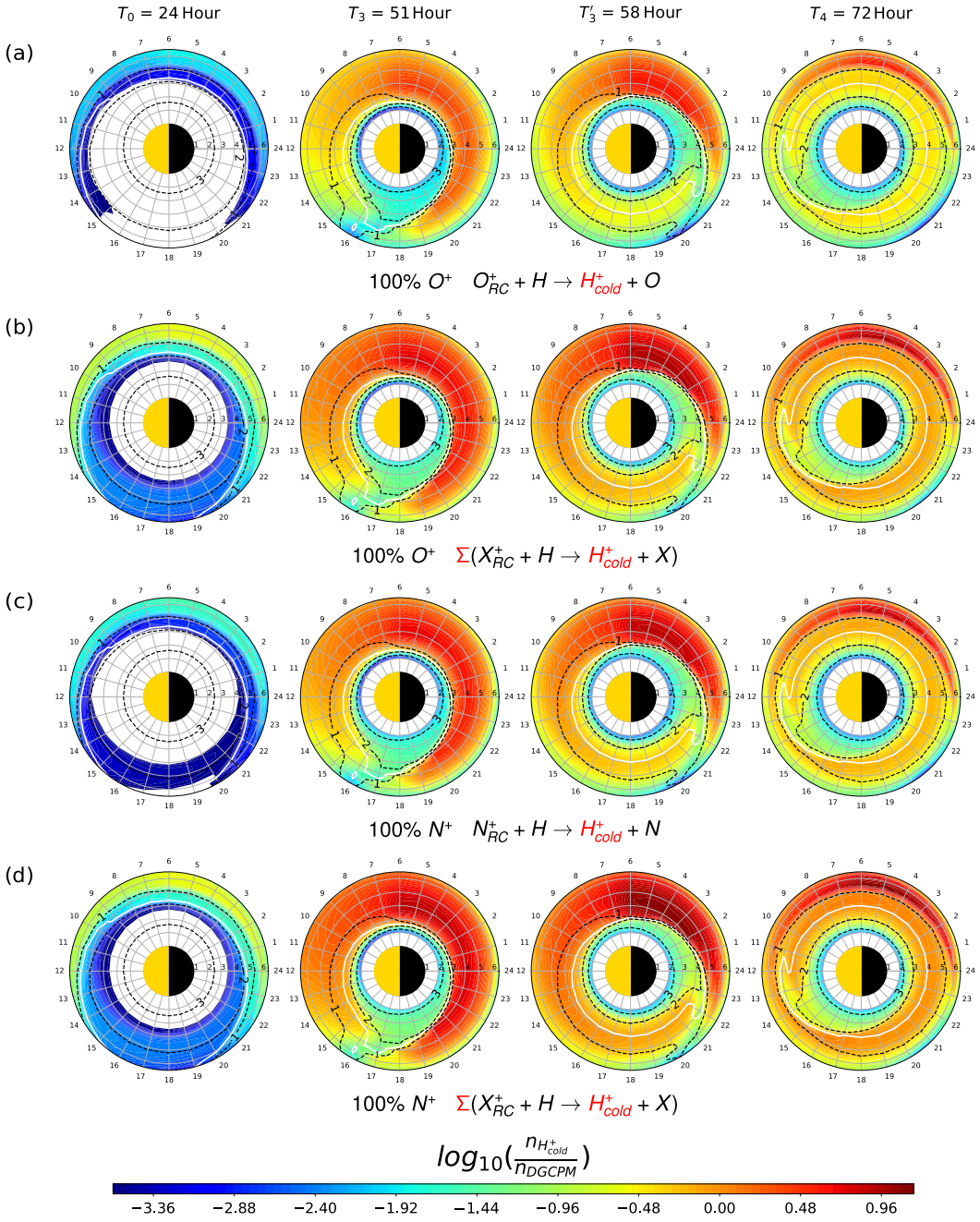

Figure 5. The density ratio (in log scale) between the charge-exchange byproduct cold H^+ highlighted by the red text at the bottom of each row, and the plasmaspheric thermal plasma predicted by Ober et al. (1997) model. The black dashed contours represent the density levels of Ober et al. (1997) model (in log scale), and the white solid contour marks constant density level of 30 cm^{-3}. The symmetric Rairden et al. (1986) model is used.